

# Incoherent Pion Production in Neutrino - Deuteron Reactions

Jia-Jun Wu,<sup>1</sup> T. Sato,<sup>2</sup> and T.-S. H. Lee<sup>1</sup>

<sup>1</sup>*Physics Division, Argonne National Laboratory, Argonne, Illinois 60439, USA*

<sup>2</sup>*Department of Physics, Osaka University, Toyonaka, Osaka 560-0043, Japan*

## Abstract

Within the multiple scattering formulation, the incoherent pion production in neutrino-deuteron reactions at energies near the  $\Delta(1232)$  resonance is investigated. The calculations include an impulse term and one-loop contributions from nucleon-nucleon ( $NN$ ) and pion-nucleon ( $\pi N$ ) final state interactions. The input amplitudes of  $\pi N$  scattering and electroweak pion production reaction on the nucleon are generated from a dynamical model which describes very extensive data of  $\pi N$  scattering and both the electromagnetic and the weak pion production reactions on the nucleon. The  $NN$  scattering amplitudes are generated from the Bonn potential. The validity of the calculational procedures is established by giving a reasonably good description of the data of pion photo-production on the deuteron. The constructed model is then applied to predict the cross sections of  $\nu + d \rightarrow \mu^- + \pi^+ + n + p$  and  $\nu + d \rightarrow \mu^- + \pi^0 + p + p$  reactions. The importance of including the  $NN$  final state interactions to understand the experimental data of these neutrino-deuteron reactions is demonstrated. Our results strongly suggest that the spectator approximation used in the previous analyses to extract the pion production cross sections on the nucleon from the data on the deuteron is not valid for the  $\nu + d \rightarrow \mu^- + \pi^+ + n + p$ , but is a good approximation for  $\nu + d \rightarrow \mu^- + \pi^0 + p + p$ .

PACS numbers: 14.20.Jn, 13.75.Jz, 13.60.Le, 13.30.Eg

## I. INTRODUCTION

A precise knowledge of neutrino-nucleus reactions is crucial in determining the properties of neutrinos and neutrino interactions, such as the mass hierarchy of neutrinos and CP violation in the lepton sector, from the data of recent and forthcoming experiments on nuclear targets[1–6]. In the region of a few GeV neutrino energy where the  $\Delta(1232)$  resonance plays an important role, quasi-elastic knock out of nucleons and incoherent single pion production processes are the main reaction mechanisms of the neutrino-nucleus reactions. Thus, the starting point of analyzing the neutrino-nucleus reactions in this energy region is a theoretical model which can describe the cross sections of the neutrino-induced single pion production on proton ( $p$ ) and neutron ( $n$ ). These cross sections had been obtained from the experiments on hydrogen and deuterium targets at Argonne National Laboratory (ANL), and Brookhaven National Laboratory (BNL) and by European Organization for Nuclear Research (BEBC-CERN) [7–14]. Various theoretical models[15–22] have been constructed by fitting these data in recent years. The uncertainties of these models can bring systematic errors in the neutrino properties determined from applying these models to analyze the neutrino-nucleus reaction data. Parts of these theoretical uncertainties could also originate from the about 30%-40% differences between the ANL and BNL data, as discussed[17, 23]. However, it seems that this problem has been resolved[24, 25].

The cross sections of neutrino-induced single pion production on the proton target can be best obtained from the measurements on the hydrogen target. In practice these cross sections were also extracted from the analysis [7–13] of the combined data from the measurements on both the hydrogen and the deuterium targets. The essential assumption of these analyses is that in the region near the peak of the quasi-free nucleon knock out process, one of the nucleons in the deuteron does not participate in the reaction mechanism and can be treated as a spectator in evaluating the cross sections on the deuteron target. With the same procedure, the cross sections of the single pion production on the neutron target were also extracted from the data on the deuteron target. In this work we examine the extent to which this spectator approximation procedure is valid.

We consider the incoherent single pion production reaction on the deuteron owing to the charged currents:  $\nu + d \rightarrow l^- + \pi^+ + p + n(\text{CC}1\pi^+)$  and  $\nu + d \rightarrow l^- + \pi^0 + p + p(\text{CC}1\pi^0)$ . If the nuclear effects, such as those owing to the nucleon Fermi motion in the deuteron and the final  $\pi NN$  interactions, are neglected, the mechanisms of this reaction can be written as

$$\nu_\mu + d \rightarrow \mu^- + \pi^+ + p + n_s \quad (1)$$

$$\rightarrow \mu^- + \pi^+ + n + p_s \quad (2)$$

$$\rightarrow \mu^- + \pi^0 + p + p_s \quad (3)$$

where  $n_s$  ( $p_s$ ) denotes that the neutron (proton) in the deuteron is assumed to be the spectator of the reaction processes. One then expects that the cross sections for three channels on the  $p$  and  $n$  can be extracted from the data on the deuteron target. Thus  $\text{CC}1\pi^0$  (Eq.(3)) will give information on  $\nu + n \rightarrow l^- + p + \pi^0$ , while  $\text{CC}1\pi^+$  (Eqs.(1)-(2)) will give information on  $\nu + p \rightarrow l^- + p + \pi^+$  and  $\nu + n \rightarrow l^- + n + \pi^+$ . However, there is no obvious reason to justify the neglect of the  $\pi NN$  final state interactions. It is natural to ask whether the extracted cross sections, in particular the cross sections on the neutron target, have the accuracy needed to constraint a model for determining the neutrino properties from analyzing the data of neutrino-nucleus reactions. The purpose of this paper is to investigate

this important question of current interest. This is also needed to understand the origins of the difficulties, such as those reported recently in Refs.[21, 22], in obtaining a fully consistent theoretical explanation of the cross sections on both the proton and the neutron targets.

To proceed, we need to start with a model which can describe the electroweak single pion production on the nucleon in the  $\Delta$  (1232) resonance region. Among the recent models of neutrino induced pion production reactions [15–22], we adopt a dynamical model developed in Refs. [15, 16, 26] (called SL model). This reaction model is defined by an energy independent Hamiltonian which has vertex interactions describing the  $\Delta$  (1232) excitation and non-resonant meson-exchange mechanisms derived from phenomenological Lagrangians by using[26, 27] a unitary transformation method. By solving the scattering equations derived from the constructed Hamiltonian, the resulting reaction amplitudes satisfy unitary condition. The SL model has been well tested[26] against the data of  $\pi N$  scattering and electromagnetic pion production reactions on the nucleon in the  $\Delta$  (1232) resonance region. It also describes[15] well the cross sections of neutrino-induced single pion production on  $p$  and  $n$  from ANL, BNL, and BEBC-CERN. The advantage of using the SL model is that we can generate both the electromagnetic and the neutrino-induced pion production amplitudes within the same theoretical framework. Because these two amplitudes contain the same vector current mechanisms, the application of this model to investigate the neutrino-induced reactions on nuclear targets, such as the deuteron considered in this work, can be first tested against the available data of reactions induced by photons and electrons.

By using the SL model and the high precision Bonn nucleon-nucleon potential[28], we have developed a method for calculating the cross sections of incoherent electroweak pion production on the deuteron within the well-studied multiple scattering theories[29–31]. Our calculations include an impulse term and one-loop contributions from nucleon-nucleon ( $NN$ ) and pion-nucleon ( $\pi N$ ) final state interactions. We first establish our calculation procedures by showing that the available data of incoherent pion photo-production reaction on the deuteron can be described reasonably well. Our results are fairly consistent with those from the earlier works[32–36] on this reaction, as discussed later. Thus the developed calculation procedures can be used reliably to investigate the  $\pi NN$  final state interaction effects on the cross sections of neutrino-induced single pion production reactions on deuteron.

In Sec. II, we recall the formula for calculating the cross sections of electroweak reactions on hadron targets. Our procedures for calculating the incoherent pion production amplitudes for the deuteron target are described in Sec. III. In Sec. IV we test our approach by investigating the pion photo-production reactions on the deuteron. Our results for the neutrino-induced pion production reactions on the deuteron are presented in Sec. V. A summary and discussions are given in Sec. VI.

## II. FORMULATION FOR THE ELECTROWEAK REACTIONS ON HADRONS

The formula for calculating the cross sections of electroweak reactions on a hadron target have been well developed in the literature[39]. For calculations on a nuclear target, it is more convenient to choose the non-covariant normalization of states:  $\langle \vec{p} | \vec{p}' \rangle = \delta(\vec{p} - \vec{p}')$  for plane wave states, and  $\langle \Phi_B | \Phi_B \rangle = 1$  for bound states. The cross sections of neutrino-induced reactions owing to charged-current (CC) can then be written

$$\frac{d\sigma}{d\Omega dE_{l'}} = \left( \frac{G_F V_{ud}}{\sqrt{2}} \right)^2 \frac{1}{4\pi^2} \frac{|\vec{p}_{l'}|}{|\vec{p}_l|} L^{\mu\nu} W_{\mu\nu}, \quad (4)$$

where  $G_F = 1.166 \times 10^{-5} GeV^{-2}$  is the Fermi coupling constant and  $V_{ud} = \cos \theta_c = 0.974$  with  $\theta_c$  being the Cabibbo angle. The lepton tensor  $L^{\mu\nu}$  depends only on the momenta of the initial neutrino ( $p_l$ ) and the final lepton ( $p_{l'}$ )

$$L^{\mu\nu} = 2[p_l^\mu p_{l'}^\nu + p_{l'}^\nu p_l^\mu - g^{\mu\nu}((p_l \cdot p_{l'}) - m_l m_{l'}) + i\epsilon^{\mu\nu\alpha\beta} p_{l,\alpha} p_{l',\beta}], \quad (5)$$

with  $\epsilon^{0123} = 1$ . The hadron tensor is defined as

$$W^{\mu\nu} = \sum_i \sum_f (2\pi)^6 \frac{E_T}{M_T} \delta^4(p_i + q - p_f) \langle f | J^\mu(0) | i \rangle \langle f | J^\nu(0) | i \rangle^* \quad (6)$$

where  $E_T$  and  $M_T$  are the energy and mass of the target hadron,  $p_i$  and  $p_f$  are the four-momenta of the initial and final states, respectively, and  $\sum_i \sum_f$  the average over the initial spin of the target and the sum over the final spins of outgoing particles.

As a comparison, we also write here the formula of electron scattering cross section:

$$\frac{d\sigma}{d\Omega dE_{l'}} = \left(\frac{4\pi\alpha}{Q^2}\right)^2 \frac{1}{4\pi^2} \frac{|\vec{p}_{l'}|}{|\vec{p}_l|} L^{\mu\nu} W_{\mu\nu}, \quad (7)$$

where  $W_{\mu\nu}$  is the same hadron tensor defined in Eq.(6), and  $\alpha = 1/137$  is the fine structure constant and  $Q^2 = -q^2$  with  $q = p_l - p_{l'}$ . The lepton tensor  $L^{\mu\nu}$  is written as

$$L^{\mu\nu} = \frac{1}{2} [p_l^\mu p_{l'}^\nu + p_{l'}^\nu p_l^\mu - g^{\mu\nu}((p_l \cdot p_{l'}) - m_l^2)]. \quad (8)$$

It is well known [39] that the inclusive differential cross sections of electron and neutrino induced reactions can be expressed in terms of structure functions  $W_i$ . In the limit of vanishing lepton mass  $m_l \sim 0$ , the double differential cross section of inclusive electron scattering ( $e + d \rightarrow e' + X$ ) is given as

$$\frac{d^2\sigma}{dE' d\Omega'} = \frac{4\alpha^2 E'^2}{Q^4} [2W_1^{em} \sin^2 \theta + W_2^{em} \cos^2 \theta]. \quad (9)$$

Here  $\theta$  and  $E'$  are the scattering angle and the energy of the final electron in the target rest frame. The cross section of the charged current neutrino reaction ( $\nu/\bar{\nu} + d \rightarrow l'(\bar{l}') + X$ ) is given as

$$\frac{d^2\sigma}{dE' d\Omega'} = \frac{(G_F V_{ud})^2 E'^2}{2\pi^2} [2W_1^{CC} \sin^2 \theta + W_2^{CC} \cos^2 \theta \pm W_3^{CC} \frac{\epsilon + \epsilon'}{M_T} \sin^2 \theta]. \quad (10)$$

Here the structure functions  $W_i$  are defined as

$$W_1^\alpha = \frac{1}{2} (W^{\alpha 11} + W^{\alpha 22}) \quad (11)$$

$$W_2^\alpha = \frac{Q^2}{\vec{q}^2} [W_1^\alpha + \frac{Q^2}{\vec{q}_c^2} W^{\alpha 00}] \quad (12)$$

$$W_3^\alpha = -\frac{2M_T}{|\vec{q}|} \text{Im}(W^{\alpha 12}), \quad (13)$$

where  $W^{\alpha 11}$ ,  $W^{\alpha 22}$ ,  $W^{\alpha 00}$  and  $W^{\alpha 12}$  are the components of the hadron tensor defined by Eq.(6) and are evaluated by using the electromagnetic current  $J_{em}^\mu$  and weak charged current  $J^\mu = V^\mu - A^\mu$  for  $\alpha = em$  and  $CC$ , respectively. We use  $J^0 + \frac{\omega_c}{Q^2} J \cdot q$  to take into account the

non-conservation of the axial vector current in place of  $J^0$  in  $W^{00}$  for the neutrino reaction. The direction of the momentum transfer is chosen to be the  $z$  direction: i.e.,  $q^\mu = (\omega, 0, 0, |\vec{q}|)$  in the target rest frame and  $q^\mu = (\omega_C, 0, 0, |\vec{q}_C|)$  in the center of mass frame of lepton and target. One can show that the total cross sections of the reactions induced by photons can be calculated only from the transverse parts of hadron tensor defined by Eq.(11):

$$\sigma^{tot} = \frac{4\pi^2\alpha}{E_\gamma} W_1^{em}. \quad (14)$$

The similarity of the cross sections for the photon, electron and neutrino induced reactions, as seen in Eqs. (9)-(14), indicates that one can test the reaction models for the neutrino-induced pion production reactions by using the data of pion photo- and electro-productions.

Starting with Eqs.(4)-(8), one can also write[37, 38] the semi-inclusive cross sections in the forms similar to Eqs.(9) and (10). For the single pion electro-production reactions on the nucleon, such a form is well known[15, 26]. To provide the information which is closely related to the recent experimental initiatives[6], it is more straightforward here to take a numerical approach. We will use directly the formula Eqs.(4)-(6) to calculate the exclusive cross sections of  $\nu + d \rightarrow l + \pi + N + N$  and then obtain the semi-inclusive cross sections by integrating out the appropriate variables of the final  $\pi NN$  states. Our numerical procedure is explained in the next section.

### III. CALCULATIONS FOR THE DEUTERON TARGET

Our task is to evaluate the hadron tensor  $W^{\mu\nu}$ , defined by Eq.(6), for  $\nu(p_l) + d(p_d) \rightarrow l'(p_{l'}) + \pi(k) + N_1(p_1) + N(p_2)$  in the Laboratory frame in which the deuteron with mass  $m_d$  is at rest and thus its four-momentum is  $p_d = (m_d, \vec{0})$ . Suppressing the spin and isospin indices, the considered hadron tensor becomes

$$\begin{aligned} W^{\mu\nu} &= (2\pi)^6 \frac{E_d(\vec{p}_d)}{m_d} \int d\vec{k} d\vec{p}_1 \delta(E_d(\vec{p}_d) + q^0 - E_\pi(\vec{k}) - E_N(\vec{p}_1) - E_N(\vec{p}_2)) \\ &\times \langle \Psi_{\vec{k}, \vec{p}_1, \vec{p}_2}^{(-)} | J^\mu(0) | \Phi_d \rangle \langle \Psi_{\vec{k}, \vec{p}_1, \vec{p}_2}^{(-)} | J^\nu(0) | \Phi_d \rangle^* \end{aligned} \quad (15)$$

where  $|\Phi_d\rangle$  is the deuteron bound state, and  $|\Psi_{\vec{k}, \vec{p}_1, \vec{p}_2}^{(-)}\rangle$  the  $\pi NN$  scattering state.

To proceed, we need to define a model for describing the electromagnetic and weak reaction mechanisms of reactions on the deuteron. Such a model can be constructed by extending the usual two-nucleon Hamiltonian to include the Hamiltonian developed in the SL model. It is then straightforward to apply the well-established multiple scattering formulation[29–31] to derive formula for calculating the the current matrix elements  $\langle \Psi_{\vec{k}, \vec{p}_1, \vec{p}_2}^{(-)} | J^\nu(0) | \Phi_d \rangle$ .

Keeping only the terms up to the second order in the multiple scattering expansion, we have

$$\langle \Psi_{\vec{k}, \vec{p}_1, \vec{p}_2}^{(-)} | J^\nu(0) | \Phi_d \rangle = \langle \vec{k}, [\vec{p}_1, \vec{p}_2]_A | J^{Imp, \nu}(0) + J^{NN, \nu}(0) + J^{\pi N, \nu}(0) | \Phi_d \rangle \quad (16)$$

where  $|\vec{k}, [\vec{p}_1, \vec{p}_2]_A\rangle$  is a  $\pi NN$  plane-wave state with an anti-symmetrized  $NN$  component  $[\vec{p}_1, \vec{p}_2]_A$ . In the following subsections, we give expressions for the matrix elements of the

impulse term  $J^{Imp,\nu}(0)$ , the  $NN$  final-state interaction term  $J^{NN,\nu}(0)$ , and the  $\pi N$  final-state interaction term  $J^{\pi N,\nu}(0)$ . For each term, the corresponding reaction amplitude is the sum of the contributions from each nucleon in the deuteron. We only give the formula to calculate the contribution from the nucleon 1. The formula can then be used for the full calculations with the properly anti-symmetrized  $NN$  in the deuteron and the final  $\pi NN$  states. This procedure is tedious but straightforward, and thus is not given in the paper.

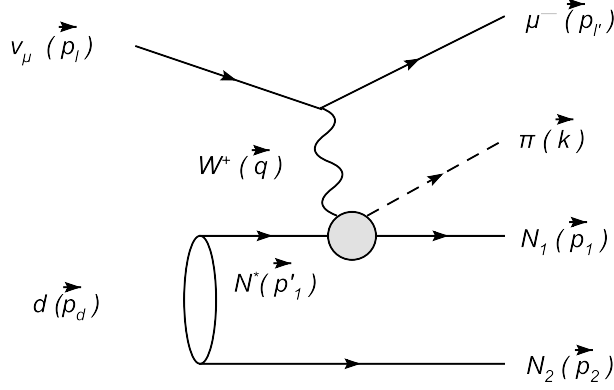


FIG. 1. Impulse mechanism  $J^{Imp,\nu}(0)$  of Eq.(17).

### A. Impulse term

With the momenta illustrated in Fig.1, the contribution from the nucleon 1 to the impulse term in the deuteron rest frame  $p_d = (m_d, \vec{0})$  can be written as

$$\langle \vec{k}, \vec{p}_1, \vec{p}_2 | J^{Imp,\nu}(0) | \Phi_d \rangle = \langle \vec{k}, \vec{p}_1 | j^\nu | \vec{q}, \vec{p}'_1 \rangle \times \Phi_d(\vec{p}_c) \quad (17)$$

where  $\vec{p}'_1 = -\vec{p}_2$ , and  $\vec{p}_c = (\vec{p}'_1 - \vec{p}_2)/2$  is the two-nucleon relative momentum, and  $j^\nu$  is either the electromagnetic or weak current associated with the nucleon 1. The current matrix element on a single nucleon in Eq.(17) is calculated[40] from

$$\begin{aligned} \langle \vec{k}, \vec{p}_1 | j^\nu | \vec{q}, \vec{p}'_1 \rangle &= \sqrt{\frac{1}{(2\pi)^9} \frac{m_N^2}{2E_\pi(\vec{k})E_N(\vec{p}_1)E_N(\vec{p}'_1)}} \\ &\times \sum_{\mu} [\Lambda_{lc}(\vec{p}_1 + \vec{k}, E_N(p_1) + E_\pi(k))]_{\mu}^{\nu} \langle \vec{\kappa} | j_c^{\mu}(W_c) | \vec{q}_c \rangle \end{aligned} \quad (18)$$

where  $\Lambda_{lc}(\vec{p}, E)$  is the Lorentz transformation for getting the current  $j^\nu$  in the laboratory frame from  $j_c^\mu$  in the center of mass system of the outgoing  $\pi N$  subsystem. The vectors  $\vec{q}_c$  and  $\vec{\kappa}$  denote the initial and final three-momentum of  $\pi$  in the center of mass system of the outgoing  $\pi N$  subsystem. Note that  $\langle \vec{\kappa} | j_c^{\mu}(W_c) | \vec{q}_c \rangle$  includes the  $\pi N$  final state interaction and thus it depends on the invariant mass  $W_c$  of the  $\pi N$  subsystem. By using the three-body approximation developed in Ref.[31], the invariant mass  $W_c$  in Eq.(18) is calculated from the energy available to the  $\pi + N$  subsystem. It is calculated from subtracting the energy

$E_N(p_2)$  of the second nucleon in Fig.1 from the total energy  $\omega + m_d$  of the initial  $W^+ + d$  system :

$$W_c = [(\omega + m_d - E_N(p_2))^2 - (\vec{p}_1 + \vec{k})^2]^{1/2} \quad (19)$$

We define the Lorentz transformation in Eq.(18) by using the momenta of the outgoing  $\pi N$  subsystem. Explicitly, we have

$$\Lambda_{lc}(\vec{p}, E) = \begin{pmatrix} \frac{E}{M} & -\frac{p_x}{M} & -\frac{p_y}{M} & -\frac{p_z}{M} \\ -\frac{p_x}{M} & 1 + \frac{p_x^2}{M(M+E)} & \frac{p_x p_y}{M(M+E)} & \frac{p_x p_z}{M(M+E)} \\ -\frac{p_y}{M} & \frac{p_y p_x}{M(M+E)} & 1 + \frac{p_y^2}{M(M+E)} & \frac{p_y p_z}{M(M+E)} \\ -\frac{p_z}{M} & \frac{p_z p_x}{M(M+E)} & \frac{p_z p_y}{M(M+E)} & 1 + \frac{p_z^2}{M(M+E)} \end{pmatrix}. \quad (20)$$

where  $M = [E^2 - \vec{p}^2]^{1/2}$ . The inverse  $[\Lambda_{lc}]^{-1}(\vec{p}, E) = \Lambda_{cl}(\vec{p}, E)$  is used to get the vector  $q_c^\mu = (\omega_c, \vec{q}_c)$  from  $q^\mu = (\omega, \vec{q})$ , and  $\kappa^\mu = (E_\pi(\vec{\kappa}), \vec{\kappa})$  from  $k^\mu = (E_\pi(\vec{k}), \vec{k})$ . We thus have

$$q_c^\nu = \sum_{\mu} [\Lambda_{cl}(\vec{p}_1 + \vec{k}, E_N(p_1) + E_\pi(k))]_{\mu}^{\nu} q^\mu \quad (21)$$

$$\kappa^\nu = \sum_{\mu} [\Lambda_{cl}(\vec{p}_1 + \vec{k}, E_N(p_1) + E_\pi(k))]_{\mu}^{\nu} k^\mu \quad (22)$$

where

$$\Lambda_{cl}(\vec{p}, E) = \begin{pmatrix} \frac{E}{M} & \frac{p_x}{M} & \frac{p_y}{M} & \frac{p_z}{M} \\ \frac{p_x}{M} & 1 + \frac{p_x^2}{M(M+E)} & \frac{p_x p_y}{M(M+E)} & \frac{p_x p_z}{M(M+E)} \\ \frac{p_y}{M} & \frac{p_y p_x}{M(M+E)} & 1 + \frac{p_y^2}{M(M+E)} & \frac{p_y p_z}{M(M+E)} \\ \frac{p_z}{M} & \frac{p_z p_x}{M(M+E)} & \frac{p_z p_y}{M(M+E)} & 1 + \frac{p_z^2}{M(M+E)} \end{pmatrix}. \quad (23)$$

As reviewed in Ref.[40], we can calculate the current matrix element in the right-hand-side of Eq.(18) by the relation

$$-\frac{m_N}{4\pi W_c} \langle \vec{\kappa} | j^\mu(W_c) | \vec{q}_c \rangle = \sum_n F_n(W_c) O_n(\hat{\kappa}, \hat{q}_c, \epsilon^\mu) \quad (24)$$

where  $F_n(W_c)$  is the Chew-Goldberger-Low-Nambu (CGLN) amplitudes, and  $O_n(\hat{\kappa}, \hat{q}_c, \epsilon^\mu)$  are the operators in the nucleon spin-space which can be found in the appendix of Ref.[40]. We generate the CGLN amplitudes  $F_n(W_c)$  from the SL model[15, 26].

## B. $NN$ final-state interaction term

In the deuteron rest frame, the matrix element of the  $NN$  final-state interaction term, as illustrated in Fig.2, can be written as

$$\begin{aligned} \langle \vec{k}, \vec{p}_1, \vec{p}_2 | J^{NN, \nu}(0) | \Phi_d \rangle &= \int d\vec{p}_1'' \langle \vec{p}_1, \vec{p}_2 | t_{NN}(E_N(p_1) + E(p_2)) | \vec{p}_1'', \vec{p}_2' \rangle \\ &\quad \times \frac{1}{E - E_N(p_1'') - E_N(p_2') - E_\pi(k) + i\epsilon} \\ &\quad \times \langle \vec{k}, \vec{p}_1'' | j^\nu | \vec{q}, \vec{p}_1' \rangle \Phi_d(\vec{p}_1') \end{aligned} \quad (25)$$

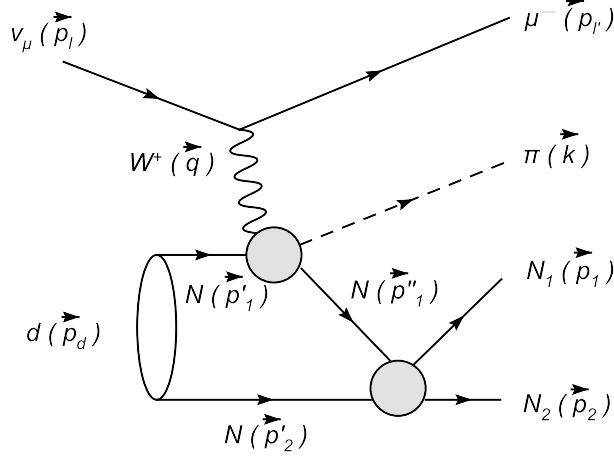


FIG. 2. The  $NN$  final state interaction term  $J^{NN,\nu}(0)$  of Eq.(25).

where  $\vec{p}'_2 = -\vec{p}'_1$ ,  $\vec{p}'_1 = \vec{p}''_1 + \vec{k} - \vec{q}$ , and the  $NN$  t-matrix is calculated from

$$\begin{aligned} & \langle \vec{p}_1, \vec{p}_2 | t_{NN}(E_N(p_1) + E_N(p_2)) | \vec{p}''_1, \vec{p}'_2 \rangle \\ &= \left[ \frac{E_N^2(p) E_N^2(p')}{E_N(p_1) E_N(p_2) E_N(p'_1) E_N(p'_2)} \right]^{1/2} \langle \vec{p} | \hat{t}_{NN}(E_c) | \vec{p}' \rangle \end{aligned} \quad (26)$$

where  $E_c = [(E_N(p_1) + E_N(p_2))^2 - (\vec{p}_1 + \vec{p}_2)^2]^{1/2}$  is the energy in the two-nucleon center of mass system,  $\vec{p}$  and  $\vec{p}'$  are the two-nucleon relative momenta calculated from  $(\vec{p}_1, \vec{p}_2)$  and  $(\vec{p}'_1, \vec{p}'_2)$ , respectively. The on- and off-shell scattering matrix elements  $\langle \vec{p} | \hat{t}_{NN}(E_c) | \vec{p}' \rangle$  in the  $NN$  center of mass system are generated from the Bonn potential. The relation Eq.(26) between the two-body matrix elements in the laboratory frame and  $NN$  center of mass frame is commonly used in multiple scattering calculations[31] and is justified in an investigation of Ref.[41, 42]. The current matrix element  $\langle \vec{k}, \vec{p}''_1 | j^\nu | \vec{q}, \vec{p}'_1 \rangle$  in the right-hand side of Eq.(25) is obtained by replacing  $\vec{p}_1$  in Eq.(18) with  $\vec{p}''_1$ . Here the invariant mass  $W_c$  is given as

$$W_c = [(\omega + m_d - E_N(p'_2))^2 - (\vec{p}''_1 + \vec{k})^2]^{1/2}. \quad (27)$$

### C. $\pi N$ final-state interaction term

With the variables given in Fig.3, the matrix element of the  $\pi N$  final state interaction term in the deuteron rest frame is

$$\begin{aligned} \langle \vec{k}, \vec{p}_1, \vec{p}_2 | J^{\pi N,\nu}(0) | \Phi_d \rangle &= \int d\vec{k}' \langle \vec{k}, \vec{p}_2 | t_{\pi N}(E_\pi(k) + E_N(p_2)) | \vec{k}', \vec{p}'_2 \rangle \\ &\quad \times \frac{1}{E - E_N(p_1) - E_N(p'_2) - E_\pi(k') + i\epsilon} \\ &\quad \times \langle \vec{k}', \vec{p}_1 | j^\nu | \vec{q}, \vec{p}'_1 \rangle \Phi_d(\vec{p}'_1) \end{aligned} \quad (28)$$

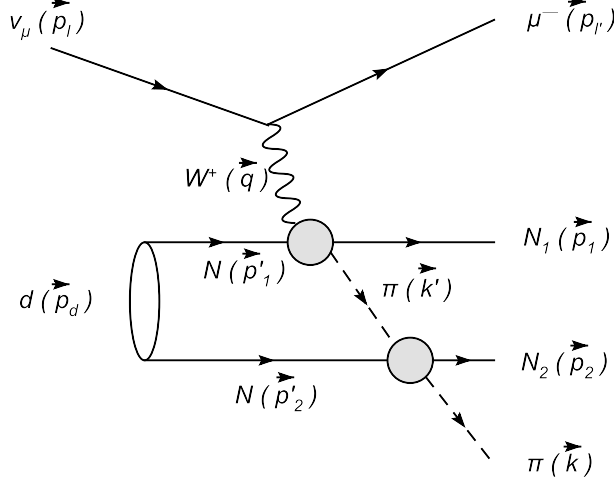


FIG. 3. The  $\pi N$  final state interaction term  $J^{\pi N, \nu}(0)$  of Eq.(28).

where  $\vec{p}'_2 = -\vec{p}'_1$ ,  $\vec{p}'_1 = \vec{p}_1 + \vec{k}' - \vec{q}$ . Similar to the relation Eq.(26), the  $\pi N$  t-matrix in Eq.(28) is calculated from

$$\langle \vec{k}, \vec{p}_2 | t_{\pi N}(E_\pi(k) + E_N(p_2)) | \vec{k}', \vec{p}'_2 \rangle = \left[ \frac{E_\pi(q_\pi) E_N(q_\pi) E_\pi(q'_\pi) E_N(q'_\pi)}{E_\pi(k) E_N(p_2) E_N(k') E_N(p'_2)} \right]^{1/2} \langle \vec{q}_\pi | \hat{t}_{\pi N}(E'_c) | \vec{q}'_\pi \rangle \quad (29)$$

where  $E'_c = [(E_\pi(k) + E(p_2))^2 - (\vec{k} + \vec{p}_2)^2]^{1/2}$  is the energy in the  $\pi N$  center of mass system,  $\vec{q}_\pi$  and  $\vec{q}'_\pi$  are the  $\pi N$  relative momenta calculated from  $(\vec{k}, \vec{p}_2)$  and  $(\vec{k}', \vec{p}'_2)$ , respectively. The current matrix element  $\langle \vec{k}', \vec{p}'_1 | j^\nu | \vec{q}, \vec{p}'_1 \rangle$  in the right-hand side of Eq.(28) is obtained by replacing  $\vec{k}$  in Eq.(18) with  $\vec{k}'$ . Here the invariant mass  $W_c$  is given as

$$W_c = [(\omega + m_d - E_N(p'_2))^2 - (\vec{p}_1 + \vec{k}')^2]^{1/2}. \quad (30)$$

#### IV. TEST OF THE MODEL IN $\gamma + d \rightarrow N + N + \pi$

To carry out the calculations using the formula described in the previous sections, we use the SL model to generate the current matrix elements  $\langle \kappa | j^\mu | q_c \rangle$  and the  $\pi N$  scattering t-matrix  $\langle q'_\pi | t_{\pi N} | q_\pi \rangle$ . The Bonn potential[28] is used to generate the  $NN$  t-matrix  $\langle \vec{p} | t_{NN} | \vec{p}' \rangle$  and the deuteron wave function  $\phi_d(\vec{p})$ . Thus there is no free parameter in our calculations. To make realistic predictions of  $\nu + d \rightarrow l + \pi + N + N$  reactions, it is necessary to test our approach by examining the extent to which the available data of  $\gamma + d \rightarrow \pi^- + p + p, \pi^0 + n + p$  can be described. Our calculations for this reaction are similar to those of Refs.[32–36], while there are differences between different approaches in the formulation and the input to the calculations.

In addition to the total cross section defined by Eq.(14), we also compare our predictions with the data of the differential cross sections. We can derive from Eq.(14) the differential cross sections in the  $\gamma$ -d center of mass frame. Including spin and isospin variables explicitly,

we have

$$\frac{d\sigma}{d\Omega_\pi} = \int dM_{NN} \frac{4\pi^2\alpha}{2E_\gamma} (\tilde{W}_{11} + \tilde{W}_{22}) \quad (31)$$

where the  $\tilde{W}_{\mu\nu}$  can be calculated from  $W_{\mu\nu}$  in Eq. (15) :

$$\begin{aligned} \tilde{W}_{\mu\nu} &= \frac{dW_{\mu\nu}}{d\Omega_\pi dM_{NN}} \\ &= \frac{(2\pi)^6}{2J_d + 1} \frac{E_d(\vec{p}_d)}{m_d} \int |\vec{k}| |\vec{p}_{NN}^*| d\Omega_{NN}^* \\ &\quad \sum_{M_J} \sum_{m_{s_1}} \sum_{m_{s_2}} \frac{E_N(\vec{p}_1) E_N(\vec{p}_2) E_\pi(\vec{k})}{\omega + m_d - \frac{E_\pi(\vec{k})q}{|\vec{k}|} \cos\theta_\pi} \\ &\quad \times \langle \vec{k} [\vec{p}_1 m_{s_1} m_{\tau_1}, \vec{p}_2 m_{s_2} m_{\tau_2}]_A | J_\mu(0) | \Phi_d^{JM_J, TM_T} \rangle \\ &\quad \times \langle \vec{k} [\vec{p}_1 m_{s_1} m_{\tau_1}, \vec{p}_2 m_{s_2} m_{\tau_2}]_A | J_\nu(0) | \Phi_d^{JM_J, TM_T} \rangle^* \end{aligned} \quad (32)$$

where  $J^\mu(0)$  is the electromagnetic current. In the above equation,  $\vec{p}_{NN}^*$  and  $\Omega_{NN}^*$  are the momentum and angle of the nucleon 1 in the rest frame of the outgoing  $NN$  system. Here we integrate out the solid angle  $\Omega_{NN}^*$ ;  $\omega$  and  $q$  are the energy and three-momentum of the momentum-transfer  $q^\mu = (\omega, 0, 0, q)$  to the deuteron;  $(m_{s_i}, m_{\tau_i})$  are the z-components of the spin and isospin of the  $i$ -th nucleon, and  $(JM_J, TM_T)$  denote the spin and isospin quantum numbers of the deuteron. For the considered photo-production reaction, we obviously have  $\omega = q$ . Note that the  $NN$  in the final  $\pi NN$  state is anti-symmetrized:

$$[[\vec{p}_1 m_{s_1} m_{\tau_1}, \vec{p}_2 m_{s_2} m_{\tau_2}]_A \rangle = \frac{1}{\sqrt{2}} [[\vec{p}_1 m_{s_1} m_{\tau_1}, \vec{p}_2 m_{s_2} m_{\tau_2} \rangle - [\vec{p}_2 m_{s_2} m_{\tau_2}, \vec{p}_1 m_{s_1} m_{\tau_1} \rangle] \quad (33)$$

The deuteron wave function in Eq.(32) is (in the deuteron rest frame)

$$\begin{aligned} |\Phi_d^{JM_J, TM_T} \rangle &= \sum_{m_{s_1} m_{\tau_1}} \sum_{m_{s_2} m_{\tau_2}} \int d\vec{p} |\vec{p} m_{s_1} m_{\tau_1}; -\vec{p} m_{s_2} m_{\tau_2} \rangle \left[ \sum_{L=0,2} \langle JM_J | L S M_L M_S \rangle \right. \\ &\quad \left. \times \langle S M_S | 1/2 1/2 m_{s_1} m_{s_2} \rangle \langle T M_T | 1/2 1/2 m_{\tau_1} m_{\tau_2} \rangle Y_{L M_L}(\hat{p}) \right] \end{aligned} \quad (34)$$

where  $S$  ( $S = 1$ ) and  $L$  are the spin and the orbital angular momentum of two nucleons, respectively. We note here that Eqs.(32) is independent of lepton kinematical variables except the momentum-transfer  $q = l_p - l'_p = (\omega, \vec{q})$ . Thus it can also be used in our later calculations of  $\nu + d \rightarrow l' + \pi + N + N$  by simply using the weak currents to evaluate the matrix elements of  $J^\nu(0)$  in Eq.(32).

Our results for the total cross sections of  $\gamma + d \rightarrow \pi^0 + n + p$  are shown in Fig.4. When only the impulse term  $J^{Imp, \nu}$  is included, we obtain the dashed curve. It is greatly reduced to the dot-dashed curve when the  $np$  final state interaction term  $J^{NN, \nu}$  is added in the calculation. When the  $\pi N$  final state interaction term  $J^{\pi N, \nu}$  is also included in our full calculation, we obtain the solid curve. Clearly, the  $np$  re-scattering effects are very large while the  $\pi N$  re-scattering give negligible contributions. In Fig. 5 we see that the  $\pi^0 np$  re-scattering effects bring the differential cross sections of  $\gamma + d \rightarrow \pi^0 + n + p$  calculated from keeping only the impulse term (dashed curves) to values (solid curves) which are in reasonable agreement with the data.

Similar comparisons for the total cross sections and differential cross sections for  $\gamma + d \rightarrow \pi^- + p + p$  are shown in Fig.6 and 7, respectively. Here we see that both the  $pp$  and the  $\pi N$  final state interactions are weak in this process. Comparing these results with those shown in Figs.4 and 5, we see the large difference between  $np$  and  $pp$  final state interactions. This finding is consistent with what was reported in the previous investigations[32–36]. It perhaps can be understood qualitatively from the properties of the initial deuteron wave function and the final  $NN$  wave functions. We first observe that the final  $\pi NN$  interactions are mainly attributable to the s-wave  $NN$  states in the considered energy region. For  $\pi^0 np$  final state, the dominant final  $np$  state is  ${}^3S_1 + {}^3D_1$  which has the same quantum number as the initial deuteron state. Because the radial wave functions of the deuteron and the scattering state in this partial wave must be orthogonal to each other, one expects that the loop integrations over these two wave functions are strongly suppressed compared with those from the impulse approximation calculations. In the impulse approximation, the final  $np$  state is not orthogonal to the deuteron wave function. Thus, the large influence of the  $np$  re-scattering here is attributable to the elimination of the spurious coherent contribution in the impulse approximation. A similar discussion can be found in Ref. [33]. However, there is no such orthogonality relation for the  ${}^1S_0 pp$  in the  $\pi^- pp$ . Consequently the final state interaction effect in the  $\gamma + d \rightarrow \pi^0 + n + p$  is much stronger than that in the  $\gamma + d \rightarrow \pi^- + p + p$ .

We see in Figs.4 - 7 that our full calculations (solid curves) are in reasonable agreement with the data in both the shapes and magnitudes, while some improvements are still needed in the future. Thus our calculation procedure is valid for predicting the  $\nu + d \rightarrow \mu + \pi + N + N$  cross sections, as given in the next section. A more detailed study of pion photo-production processes is not relevant to our objective here, and therefore is not further discussed.

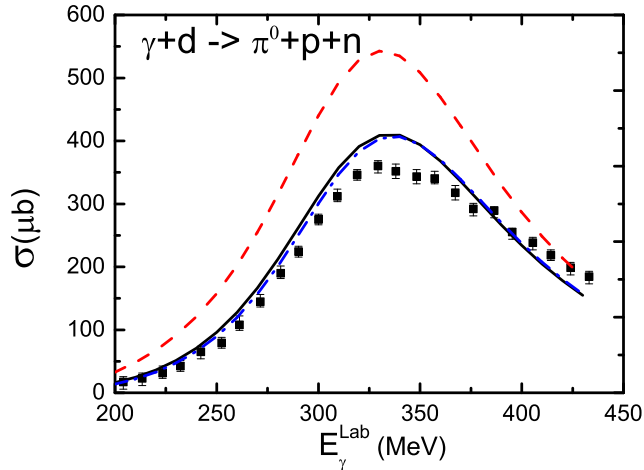


FIG. 4. (Color online) The total cross sections of  $\gamma + d \rightarrow \pi^0 + n + p$ . The red dashed, blue dash-dotted, and black solid curves represent only the impulse term, the impulse + ( $NN$  final state interaction), and the impulse + ( $NN$  final state interaction) + ( $\pi N$  final state interaction), respectively. Data are from Ref. [43].

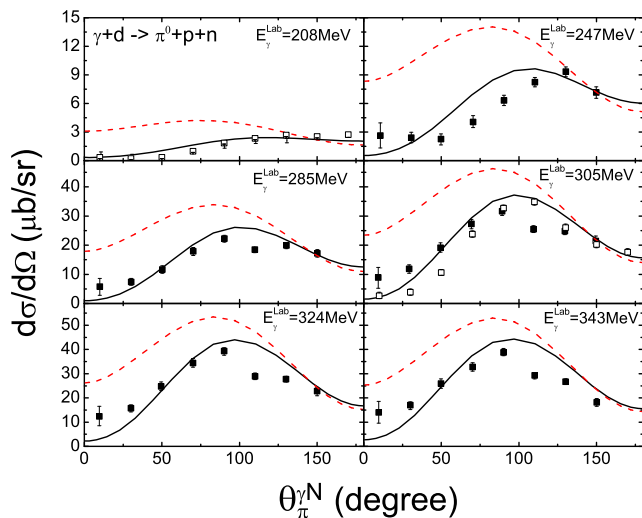


FIG. 5. (Color online) The calculated differential cross sections (solid curves) of  $\gamma + d \rightarrow \pi^0 + n + p$  are compared with the data from Ref. [43](solid boxes) and Ref. [46](open boxes). The dashed curves are from calculations including only the impulse term  $J^{Imp,\nu}(0)$ . Note that [43] the experiment data are defined in the initial  $\gamma N$  center of mass system where  $N$  is one of the nucleons which are assumed to be 'frozen' in the deuteron. This system is equivalent to a system in which the deuteron momentum  $\vec{p}_d$  is related to the photon momentum  $\vec{q}$  by  $\vec{p}_d = -2\vec{q}$ .

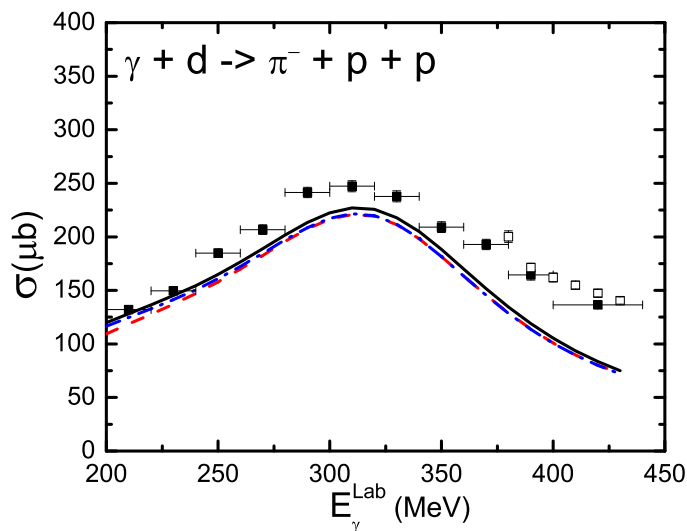


FIG. 6. (Color online) The total cross sections of  $\gamma + d \rightarrow \pi^- + p + p$ . The red dashed, blue dash-dotted, and black solid curves represent only the impulse term, the impulse + ( $N$  final state interaction), and the Impulse + ( $NN$  final state interaction) + ( $\pi N$  final state interaction), respectively. Data are from Ref. [44](Solid boxes) and Ref. [45](open boxes).

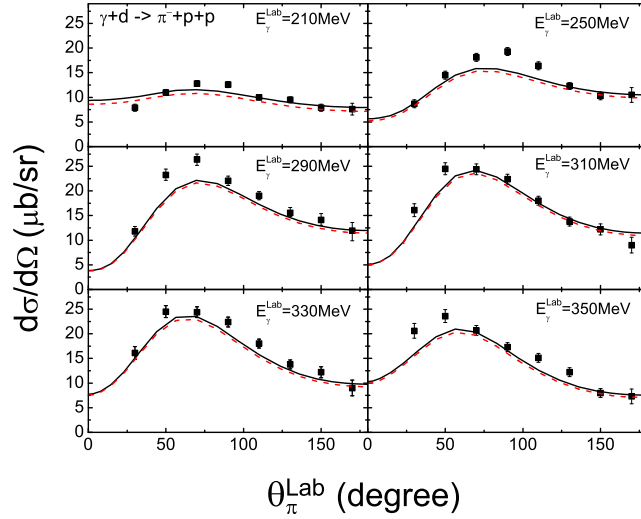


FIG. 7. (Color online) The calculated differential cross sections (solid curves) of  $\gamma + d \rightarrow \pi^- + p + p$  in the laboratory frame are compared with the data[44]. The dashed curves are from calculations including only the impulse term  $J^{Imp,\nu}(0)$ .

## V. RESULTS FOR $\nu + d \rightarrow l^- + \pi + N + N$

Following the recent experimental initiatives [6], we make predictions for the incoming muon-neutrino ( $\nu_\mu$ ) energy  $E_{\nu_\mu} = 1$  GeV. The outgoing muon energy is chosen to be  $E_{\mu^-} = 550, 600, 650$  MeV. The angle between  $\nu_\mu$  and  $\mu^-$  is set as  $\theta_{\mu^-} = 25$  degree. This kinematics is chosen to get maximum values of the predicted cross sections. The coordinate system of the laboratory system (the rest frame of the deuteron) is defined as follows: The transfer momentum  $\vec{q}$  is in the  $z$  direction and the scattering plane of incoming muon-neutrino and outgoing muon is the  $x - z$  plane.

To proceed, we first calculate the differential cross section

$$\frac{d\sigma}{dE_{\mu^-} d\Omega_{\mu^-} d\Omega_\pi dM_{NN}} = \left( \frac{G_F v_{ud}}{\sqrt{2}} \right)^2 \frac{|\vec{p}_{\mu^-}|}{|\vec{p}_\nu|} \frac{1}{4\pi^2} L^{\mu\nu} \tilde{W}_{\mu\nu}, \quad (35)$$

where  $\Omega_{\mu^-}$  and  $\Omega_\pi$  are the solid angles of outgoing muon and pion, respectively, and  $M_{NN}$  is the invariant mass of the outgoing NN system. The polar and azimuthal angles of pion  $\theta_\pi^{Lab}$  and  $\phi_\pi$  are the angles from the  $z$ -axis and the  $x$ -axis, respectively. In the following calculation for the pion angular distribution, we have chosen  $\phi_\pi = 0$ . The right-hand-side of Eq.(35) can be calculated by using  $L^{\mu\nu}$  of Eq.(5) and  $\tilde{W}_{\mu\nu}$  given in Eq.(32). By integrating the  $NN$  invariant mass  $M_{NN}$ , we then obtain semi-exclusive cross section  $\frac{d\sigma}{dE_{\mu^-} d\Omega_{\mu^-} d\Omega_\pi}$ .

Our predictions for both  $\frac{d\sigma}{dE_{\mu^-} d\Omega_{\mu^-} d\Omega_\pi}$  and  $\frac{d\sigma}{dE_{\mu^-} d\Omega_{\mu^-} d\Omega_\pi dM_{NN}}$  are presented in the following two subsections.

### A. Results of $\nu_\mu + d \rightarrow \mu^- + \pi^+ + p + n$

The predicted differential cross sections  $d\sigma/dE_{\mu^-}d\Omega_{\mu^-}d\Omega_{\pi^+}$  for  $\nu_\mu + d \rightarrow \mu^- + \pi^+ + p + n$  with  $E_\mu = 550, 600, 650$  MeV are shown in Fig.8. The red dashed curves are from the calculations including only the impulse term ( $J^{Imp,\nu}(0)$ ) in Eq.(16). When the  $NN$  final state interaction term ( $J^{NN,\nu}(0)$ ) is included, the cross sections are changed to the dot-dashed blue curves. Clearly, the  $np$  final state interactions are significant, in particular in the forward pion angles. When the  $\pi N$  final state interaction term ( $J^{\pi N,\nu}(0)$ ) term is also included, we obtain our full results denoted as solid black curves. The small differences between the dot-dashed and solid curves indicate that the  $\pi N$  final state interaction effects are negligible in this chosen kinematics. This result is similar to what we have observed in our results for  $\gamma + d \rightarrow \pi^0 + n + p$ . This is not surprising because both have the same  $np$  scattering mechanisms. From the solid black curves in Fig.8, we see that the cross section with the outgoing muon energy  $E_{\mu^-} = 600$  MeV is the largest in the considered kinematics.

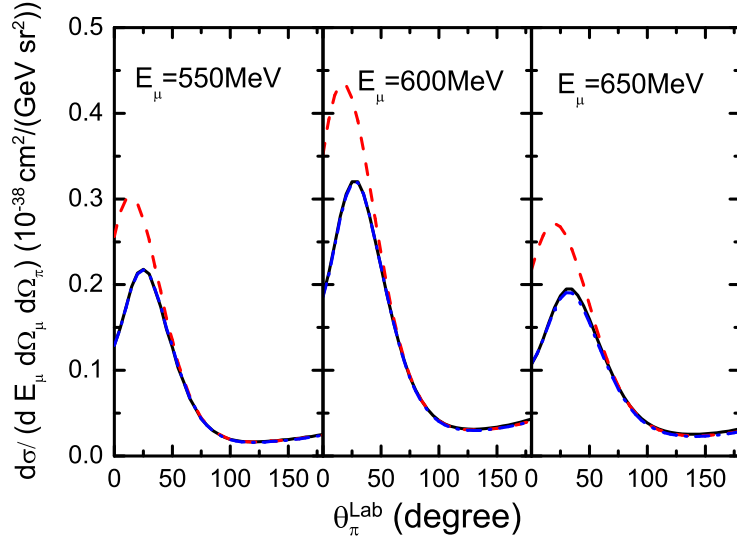


FIG. 8. (Color online) The differential cross sections  $d\sigma/dE_{\mu^-}d\Omega_{\mu^-}d\Omega_{\pi^+}$  of  $\nu_\mu + d \rightarrow \mu^- + \pi^+ + p + n$  as function of  $\theta_{\pi^+}$  in the laboratory frame at  $E_{\mu^-} = 550, 600, 650$  MeV. The red dashed, blue dash-dotted, and black solid curves represent only the impulse term, the impulse + ( $NN$  final state interaction), and the Impulse + ( $NN$  final state interaction) + ( $\pi N$  final state interaction), respectively. The blue dash-dotted and black solid curves are almost indistinguishable because the  $\pi N$  final state interaction effects are very small.

To understand the angle-dependence of the  $np$  final state interaction in Fig.8, we show the predicted  $NN$  invariant mass distributions  $d\sigma/dE_{\mu^-}d\Omega_{\mu^-}d\Omega_{\pi^+}dM_{pn}$  at  $E_\mu = 600$  MeV in Fig.9 for several outgoing pion angle  $\theta_\pi$ . For the forward angles  $\theta_\pi \leq 45^\circ$ , the  $NN$  invariant masses are near the threshold region where the  $np$  cross sections are very large and hence the effects owing to  $np$  final state interactions are large. Furthermore, we find that the shoulders near the threshold are mainly attributable to the strong attractive interaction in the  ${}^3S_1 + {}^3D_1$  partial wave of the  $pn$  subsystem. At larger angles  $\theta > 90^\circ$ , the allowed  $NN$  invariant masses are shifted to the higher mass region around 100 MeV where the  $np$  cross

sections are much smaller and hence the corresponding  $np$  final state interaction effects are much weaker.

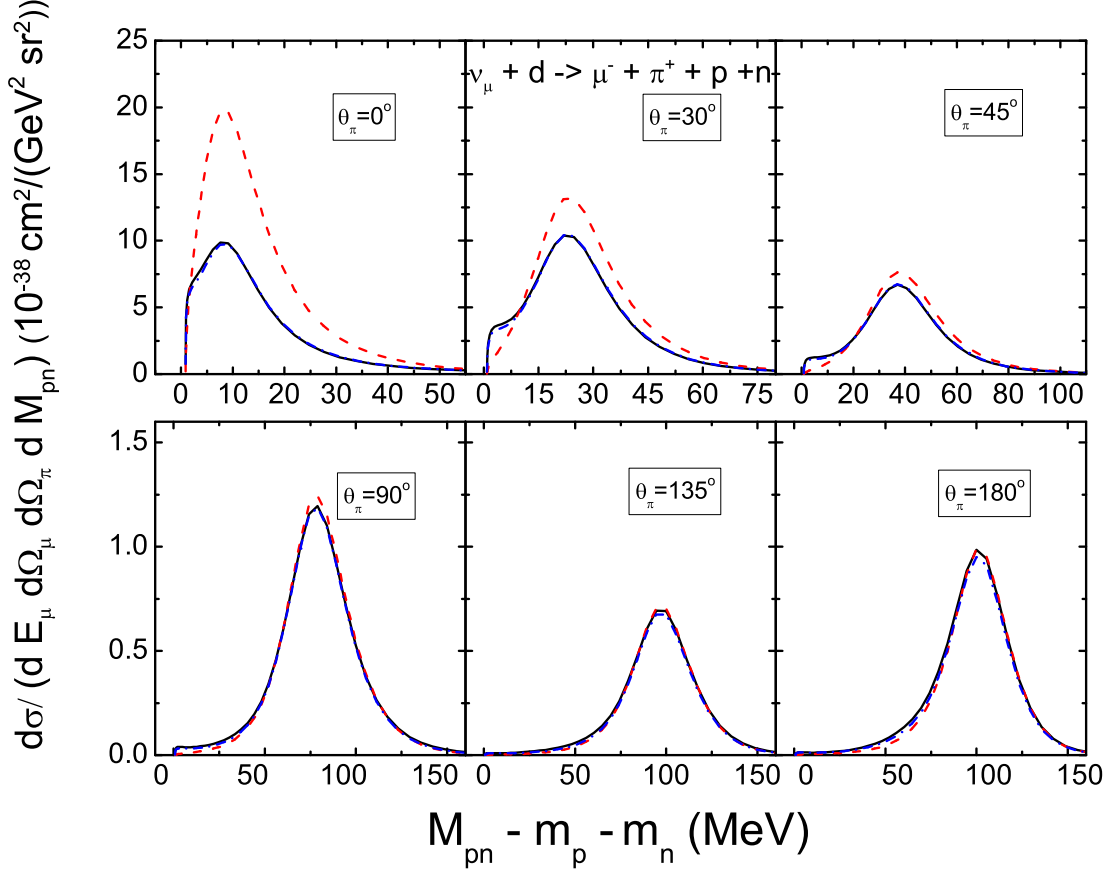


FIG. 9. (Color online) The differential cross sections  $d\sigma/dE_{\mu^-}d\Omega_{\mu^-}d\Omega_{\pi^+}dM_{pn}$  of  $\nu_{\mu} + d \rightarrow \mu^{-} + \pi^{+} + p + n$  as function of  $M_{pn}$  at several outgoing pion angles  $\theta_{\pi}$ . The outgoing muon energy is  $E_{\mu^-}=600$  MeV. The red dashed, blue dash-dotted, and black solid curves represent only the impulse term, the impulse + ( $NN$  final state interaction), and the Impulse + ( $NN$  final state interaction) + ( $\pi N$  final state interaction), respectively. The blue dash-dotted and black solid curves are almost indistinguishable because the  $\pi N$  final state interaction effects are very small.

### B. Results of $\nu_{\mu} + d \rightarrow \mu^{-} + \pi^0 + p + p$

In Fig.10, we present the predicted differential cross sections of  $d\sigma/dE_{\mu^-}d\Omega_{\mu^-}d\Omega_{\pi^0}$  of the  $\nu_{\mu} + d \rightarrow \mu^{-} + \pi^0 + p + p$  reaction. In contrast with the  $\nu_{\mu} + d \rightarrow \mu^{-} + \pi^{+} + n + p$ , we see that the results (red dashed curves) from the calculations including only the impulse term are close to the results (blue dot-dashed curves) including also the  $pp$  final state interaction. The situation here is similar to what we have observed in the preview section that the final state interaction effects from  $np$  scattering are much larger than that from  $pp$  scattering.

Comparing the dot-dashed curves and the black solid curves from our full calculations, we see that the  $\pi N$  final state interaction effects are negligible. This is also similar to what we have seen in Fig.6 for the  $\gamma + d \rightarrow \pi^- + p + p$  process. The weak  $pp$  and  $\pi N$  final state interaction effects can also be seen clearly in Fig.11 for the  $NN$  invariant mass distribution  $d\sigma/dE_{\mu^-}d\Omega_{\mu^-}d\Omega_{\pi^0}dM_{pp}$ . The only exception is that a pronounced sharp peak at the forward pion angles  $\theta_{\pi^0} = 0^\circ, 25^\circ$ . The origin of this peak can be seen in Fig.12. We see that the impulse term (red dashed curve) raises smoothly from the threshold, while the  $pp$  final interaction, which is dominated by the  $^1S_0$  partial wave in this very low energy region, generates a peak (pink dotted curve). A similar discussion has been given in Ref.[33]. The Coulomb interaction between two protons is not taken into account in the present work. Whether this peak will be modified needs to be investigated in the future.

We note that the cross sections of  $\nu + d \rightarrow \mu^- + \pi^0 + p + p$  cross section is smaller by a factor of about 4 than the  $\nu + d \rightarrow \mu^- + \pi^+ + n + p$  presented in the previous subsection. This is mainly attributable to the fact that the  $\pi^+pn$  production cross sections include  $\nu_\mu + p \rightarrow \mu^- + \pi^+ + p$  and  $\nu_\mu + n \rightarrow \mu^- + \pi^+ + n$ , while the  $\pi^0np$  production include only  $\nu_\mu + n \rightarrow \mu^- + \pi^0 + p$ . Furthermore, the cross section of  $\nu_\mu + p \rightarrow \mu^- + \pi^+ + p$  is much larger than that of other two reactions [15].

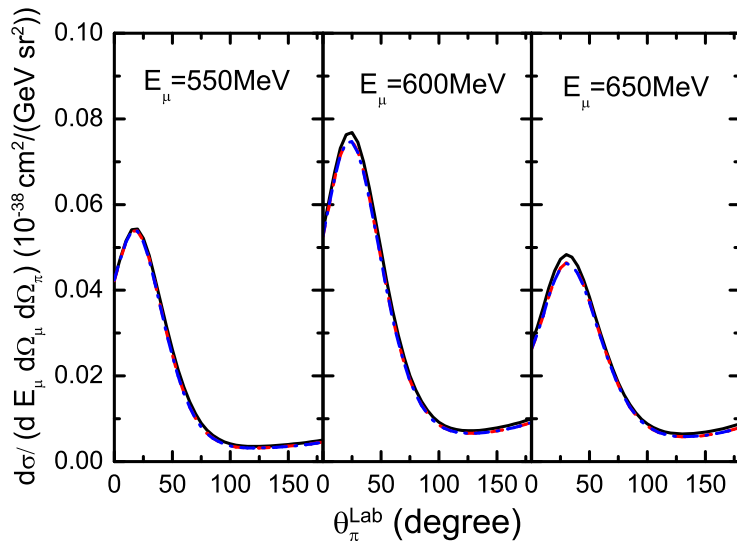


FIG. 10. (Color online) The differential cross sections  $d\sigma/dE_{\mu^-}d\Omega_{\mu^-}d\Omega_{\pi^0}$  of  $\nu_\mu + d \rightarrow \mu^- + \pi^0 + p + p$  as function of  $\theta_{\pi^0}$  in the laboratory system at  $E_{\mu^-} = 550, 600, 650$  MeV. The red dashed, blue dash-dotted, and black solid curves represent only the impulse term, the impulse + ( $NN$  final state interaction), and the Impulse + ( $NN$  final state interaction) + ( $\pi N$  final state interaction), respectively. The blue dash-dotted and black solid curves are almost indistinguishable because the  $\pi N$  final state interaction effects are very small.

### C. Extraction of nucleon cross sections from the deuteron data.

In Sec. I, we describe a procedure that was used in the previous analyses[7–13] to extract the neutrino-induced single pion production cross sections on the proton and neutron from

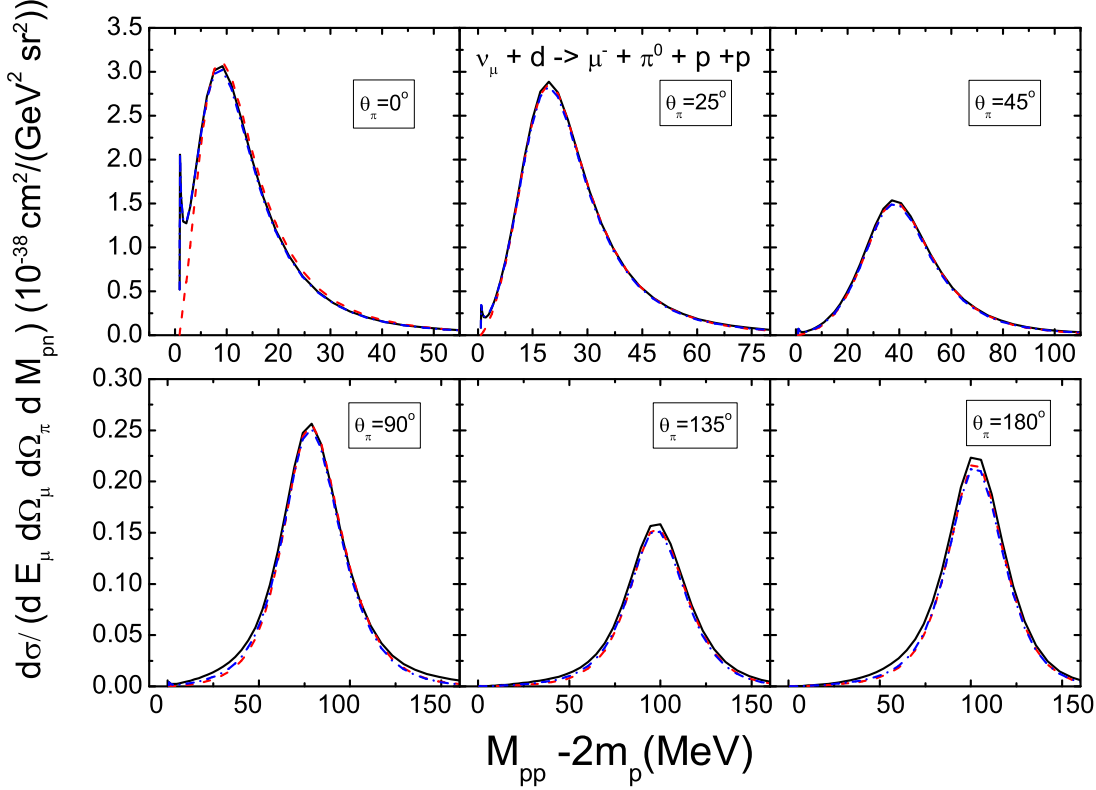


FIG. 11. (Color online) The differential cross sections  $d\sigma/dE_{\mu}-d\Omega_{\mu}-d\Omega_{\pi^0}dM_{pp}$  of  $\nu_{\mu} + d \rightarrow \mu^{-} + \pi^0 + p + p$  as function of  $M_{pp}$  in the laboratory system. The outgoing muon energy is  $E_{\mu^{-}}=600$  MeV. The red dashed, blue dash-dotted, and black solid curves represent only the impulse term, the impulse + ( $NN$  final state interaction), and the Impulse + ( $NN$  final state interaction) + ( $\pi N$  final state interaction), respectively. The blue dash-dotted and black solid curves are almost indistinguishable because the  $\pi N$  final state interaction effects are very small.

the data on the deuteron target. It is based on the assumption that in the region near the quasi-free peaks, one of the nucleons in the deuteron is simply a spectator of the reaction mechanisms. Here we use our model to examine the extent to which this procedure is valid.

To be specific, we consider the case that the spectator nucleon is at rest. If there are no final state interactions, the  $\nu + d \rightarrow l^{-} + \pi^{+} + n + p$  cross section is only from the pion production on the other nucleon which is also at rest in the deuteron rest frame. Then the cross sections measured at the kinematics where the final proton (neutron) is at rest  $\vec{p}_p = 0$  ( $\vec{p}_n = 0$ ) are simply the cross sections of  $\nu_{\mu} + n \rightarrow \mu^{-} + \pi^{+} + n$  ( $\nu_{\mu} + p \rightarrow \mu^{-} + \pi^{+} + p$ ). The cross sections for this special kinematics can be calculated from keeping only the impulse term  $J^{imp,\nu}(0)$  in Eq.(15). These are the dashed curves in Fig. 13. Here we note that the dashed curves of  $\vec{p}_n = 0$  (right) are almost one order of magnitude larger than those of  $\vec{p}_p = 0$  (left). This can be understood from the relation  $\langle \pi^{+}p | J_{CC}^{\mu} | p \rangle = 3 \langle \pi^{+}n | J_{CC}^{\mu} | n \rangle$  of the charged current contributions in the isospin  $I = 3/2$  channel which dominates the reaction cross sections in the  $\Delta(1232)$  resonance region.

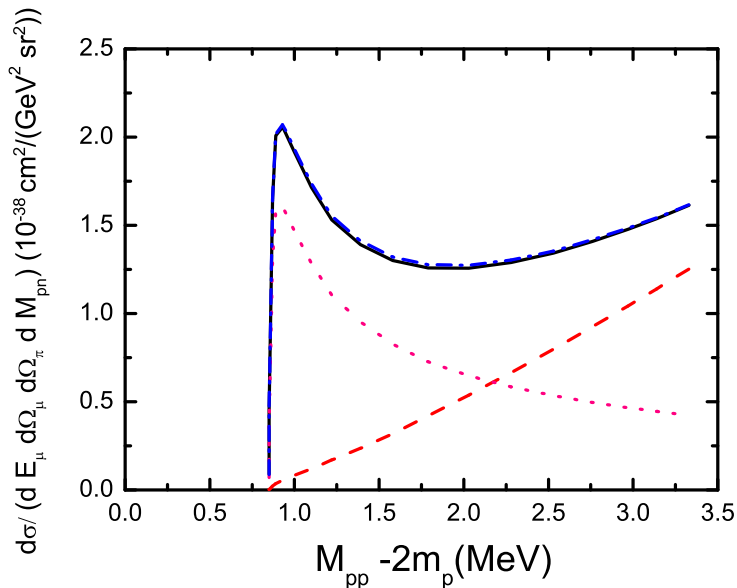


FIG. 12. The differential cross sections  $d\sigma/dE_{\mu^-}d\Omega_{\mu^-}d\Omega_{\pi^0}dM_{pp}$  of  $\nu_{\mu} + d \rightarrow \mu^{-} + \pi^0 + p + p$  as function of  $M_{pp}$  in the laboratory system. The outgoing pion angle is  $\theta_{\pi} = 0^{\circ}$ , and the outgoing muon energy is  $E_{\mu^-} = 600$  MeV. The red dashed and pink dotted curves are from calculations including only the Impulse term and only the  $NN$  final state interaction term, respectively. The blue dash-dotted and black solid curves represent the impulse + ( $NN$  final state interaction), and the Impulse + ( $NN$  final state interaction) + ( $\pi N$  final state interaction), respectively. The blue dash-dotted and black solid curves are almost indistinguishable because the  $\pi N$  final state interaction effects are very small.

When the  $NN$  final-state interaction terms are included, we obtain the dot-dashed curves in Fig. 13. The solid curves are obtained when the  $\pi N$  final state interaction is also included in the calculations. Clearly, the  $NN$  re-scattering can significantly change the cross sections while the  $\pi N$  re-scattering effects are weak. It is also important to note that the  $NN$  re-scattering effects on the cross sections for  $\vec{p}_p = 0$  are rather different than for  $\vec{p}_n = 0$ .

The results shown in Fig. 13 strongly suggest that the spectator assumption used in the previous analyses[7–13] is not valid for the CC1 $\pi^+$  process  $\nu + d \rightarrow \mu^{-} + \pi^+ + n + p$ . This result is attributable to the large  $np$  re-scattering effects, as explained in Sec. IV and V.A.

We have also examined the results for  $p_s = 0$  for the CC1 $\pi^0$  process  $\nu + d \rightarrow \mu^{-} + \pi^0 + p + p$ . Here we find that the spectator assumption is a good approximation for extracting the cross section on the nucleons from the deuteron target. This is, of course, attributable to the weak  $pp$  final state interactions, as can be seen in Fig.10.

## VI. SUMMARY AND DISCUSSIONS

We have developed an approach to predict the cross sections of electroweak pion production on the deuteron in the energy region near the  $\Delta(1232)$  resonance. Within the multiple scattering formulation[29, 30], the calculations include the impulse term and the one-loop contributions from  $NN$  and  $\pi N$  final state interactions. The current matrix elements on the

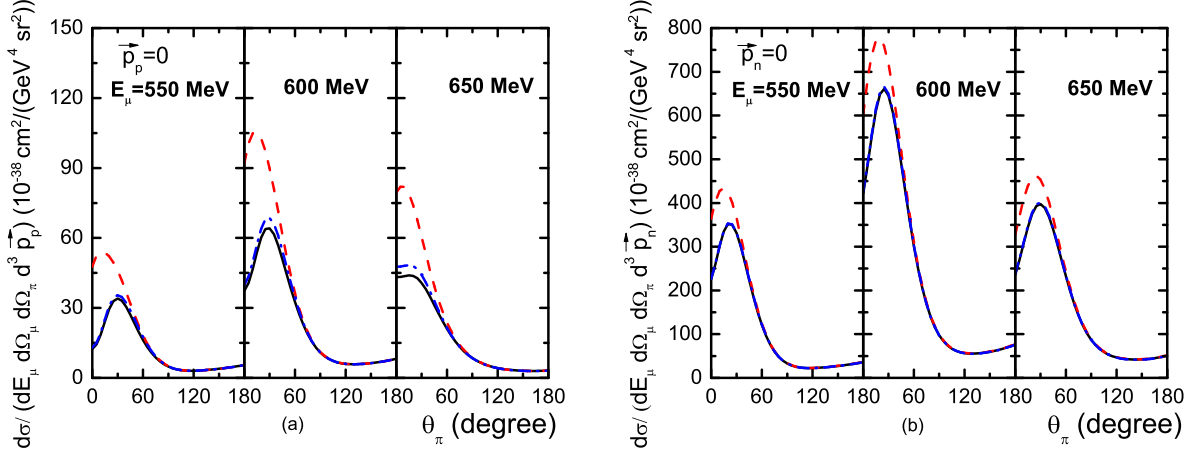


FIG. 13. (Color online) The differential cross sections  $d\sigma/dE_{\mu^-}d\Omega_{\mu^-}d\Omega_{\pi^+}d^3\vec{p}_N$  of  $\nu_{\mu} + d \rightarrow \mu^{-} + \pi^{+} + p + n$  as function of pion scattering angle in the laboratory system. Panels (a) and (b) figures are for the proton  $\vec{p}_p = 0$  and neutron  $\vec{p}_n = 0$  spectator kinematics, respectively. The outgoing muon energy is  $E_{\mu^-} = 550, 600, \text{ and } 650 \text{ MeV}$ . The red dashed, blue dash-dotted, and black solid curves are from calculations including only the Impulse term, Impulse + ( $NN$  final state interaction), and Impulse + ( $NN$  final state interaction) + ( $\pi N$  final state interaction), respectively. The blue dash-dotted and black solid curves are almost indistinguishable because the  $\pi N$  final state interaction effects are very small.

nucleon and the  $\pi N$  scattering amplitudes are generated from the SL model of electroweak pion production on the nucleon developed in Refs.[15, 26]. The  $NN$  scattering amplitudes and the deuteron bound state wave function are generated from Bonn potential[28]. There is no free parameter in the calculations.

We first test the validity of the constructed model by investigating the pion photo-production on the nucleon. The predicted cross sections are in reasonable agreement with the available data, while some further improvements are needed. The importance of the  $np$  final-state interactions is demonstrated, in agreement with the results of Ref.[32–36].

To provide information for the recent experimental initiatives[6], we make predictions for the incoming muon neutrino energy  $E_{\nu} = 1 \text{ GeV}$ . The differential cross sections for the outgoing muon energies  $E_{\mu^-} = 550, 600, 650 \text{ MeV}$  and lepton scattering angle  $\theta_{\nu, \mu} = 25^\circ$  are presented. It is found that the  $np$  final state interaction effects are very large in determining the differential cross sections of  $\nu_{\mu} + d \rightarrow \mu^{-} + \pi^{+} + n + p$  in the region where the outgoing pions are in the forward angles with respect to the incoming neutrinos. However, the  $pp$  final state interaction effect is found to be weak in the  $\nu_{\mu} + d \rightarrow \mu^{-} + \pi^0 + p + p$  except that it generates a sharp peak at energies very near the  $pp$  threshold. The  $\pi N$  final state interactions are found to be weak in both processes.

Our results strongly suggest that the spectator approximation procedure used in the previous analyses to extract the pion production cross sections on the nucleon from the data on the deuteron is not valid for the  $\nu + d \rightarrow \mu^{-} + \pi^{+} + n + p$ , but is a good approximation for  $\nu + d \rightarrow \mu^{-} + \pi^0 + p + p$ .

In the present calculations, we have not included the contributions from the exclusive  $\nu_{\mu} + d \rightarrow \mu^{-} + \pi^{+} + d$  processes. Furthermore, only the loop contributions from  $NN$

and  $\pi N$  final state interactions are included. To improve the accuracy of our predictions for analyzing future experiments on neutrino properties, it is necessary to make further developments of the model constructed in this work. It will be highly desirable to perform calculations by extending the unitary  $\pi NN$  reaction models, as reviewed in [47], to include the electroweak currents. Specifically, this can be done by extending the unitary  $\pi NN$  calculations of Ref.[48] to include the electroweak currents of the SL model[15, 26]. It will be also important to apply our approach to investigate neutrino-deuteron reactions in the higher energy region where the higher mass nucleon resonances play important roles. Such an investigation can be performed when the coupled-channel model of  $\pi N$  and  $\gamma N$  reactions developed in Ref.[49] has been extended to include weak axial currents[50]. Our effort in these directions will be reported elsewhere.

## ACKNOWLEDGMENTS

We thank B. Krusche for his help in explaining the data of Ref.[43]. This work was supported by the U.S. Department of Energy, Office of Nuclear Physics Division, under Contract No. DE-AC02-06CH11357, and JSPS KAKENHI Grant Nos. 24540273 and 25105010. This research used resources of the National Energy Research Scientific Computing Center, which is supported by the Office of Science of the U.S. Department of Energy under Contract No. DE-AC02-05CH11231, and resources provided on the Blues and/or Fusion, high-performance computing cluster operated by the Laboratory Computing Resource Center at Argonne National Laboratory.

- 
- [1] J. A. Formaggio and Z. P. Zeller, *Rev. Mod. Phys.* **84**, 1307 (2012)
  - [2] L. Alvarez-Ruso, Y. Hayato and J. Nieves, arXiv:1403.2673[hep-ph].
  - [3] K. Abe et al.(Hyper-Kamiokande working group), arXiv 1109.3262[hep-ex] (2011).
  - [4] C. Adams et al. (LBNE collaboration) arXiv:1307.7335[hep-ex] (2013).
  - [5] S. K. Agarwalla *et al.* [LAGUNA-LBNO Collaboration], *JHEP* **1405**, 094 (2014) [arXiv:1312.6520 [hep-ph]].
  - [6] M. Wilking, talk at the 9th International Workshop on Neutrino-Nucleus Interactions in the Few-GeV Region(NuInt14), 2014, Surrey (UK).
  - [7] J. Campbell et al., *Phys. Rev. Lett.* **30**, 335 (1973).
  - [8] S. J. Barish et al., *Phys. Rev.* **D19**, 2521 (1979).
  - [9] G. M. Radecky et al, *Phys. Rev.* **D25**, 1161 (1982).
  - [10] T. Kitagaki et al., *Phys. Rev.* **D34**, 2554 (1986).
  - [11] T. Kitagaki et al., *Phys. Rev.* **D42**, 1331 (1990).
  - [12] P. Allen et al., *Nucl. Phys.* **B176**, 269 (1980).
  - [13] D. Allasia et al., *Nucl. Phys.* **B343**, 285 (1990).
  - [14] G. T. Jones et al, *Z. Phys. C* **43**, 541 (1989).
  - [15] T. Sato, D. Uno and T. S. H. Lee, *Phys. Rev. C* **67**, 065201 (2003)
  - [16] T. Matsui, T. Sato and T. S. H. Lee, *Phys. Rev. C* **72**, 025204 (2005).
  - [17] E. A. Paschos, Ji-Young Yu and M. Sakuda, *Phys. Rev.* **D69**, 014013 (2004).
  - [18] O. Lalakulich and E. A. Paschos, *Phys. Rev.* **D71**, 074003 (2005).
  - [19] O. Lalakulich, E. A. Paschos and G. Piranishvili, *Phys. Rev.* **D74**, 014009 (2006).
  - [20] E. Hernandez, J. Nieves and M. Valverde, *Phys. Rev.* **D76**, 033005 (2007).
  - [21] E. Hernandez, J. Nieves, M. Valverde and M. J. Vicente Vacas, *Phys. Rev.* **D81**, 085046 (2010).
  - [22] O. Lalakulich, T. Leitner, O. Buss and U. Mosel, *Phys. Rev.* **D82**, 093001 (2010).
  - [23] M. O. Wascko (MinoBooNE Collaboration), *Nucl. Phys. B, Proc. Suppl.* **159**, 50 (2006).
  - [24] K. M. Graczyk, D. Kielczwska, P. Przewloski and J. T. Sobczyk, *Phys. Rev.* **D80**, 093001 (2009).
  - [25] C. Wilkinson, P. Rodrigues, S. Cartwright, L. Thompson and K. McFarland, *Phys. Rev. D* **90**, no. 11, 112017 (2014) [arXiv:1411.4482 [hep-ex]].
  - [26] T. Sato and T.-S. H. Lee, *Phys. Rev. C* **54**, 2660 (1996); *Phys. Rev. C* **63**, 055201 (2001).
  - [27] M. Kobayashi, T. Sato, and H. Ohtsubo, *Prog. Theor. Phys.* **98**, 927 (1997).
  - [28] R. Machleidt, in *Advances in Nuclear Physics*, edited by J.W. Negele and E. Vogt (Plenum,

- New York, 1989), Vol.19, Chap. 2.
- [29] A.K. Kerman, H. McManus, and R.M. Thaler, *Annals Phys.* **8**, 551 (1959).
  - [30] Herman Feshbach, *Theoretical Nuclear Physics: Nuclear Reactions*, John Wiley and Sons (1992).
  - [31] A. W. Thomas and R.H. Landau, *Phys.Rept.* **58**, 121 (1980).
  - [32] E. M. Darwish, H. Arenhovel and M. Schwamb, *Eur. Phys. J. A* **16**, 111 (2003).
  - [33] A. Fix and H. Arenhoevel, *Phys.Rev. C* **72**, 064005 (2005).
  - [34] M. I. Levchuk, A. Yu. Loginov, A. A. Sidorov, V. N. Stibunov and M. Schumacher, *Phys. Rev. C* **74**, 014004 (2006).
  - [35] M. Schwamb, *Phys. Rep.* **485**, 109 (2010).
  - [36] V. E. Tarasov, W. J. Briscoe, H. Gao, A. E. Kudryavtsev and I. I. Strakovsky, *Phys. Rev. C* **84**, 035203 (2011).
  - [37] T. de Forest, Jr, *Ann. Phys.* **45**, 365 (1967).
  - [38] M. Gourdin, *Nucl. Phys.* **B49**, 501 (1972).
  - [39] C. Quigg, *Gauge Theories of the Strong, Weak, and Electromagnetic Interactions: Second Edition*, Princeton University Press (2013).
  - [40] T. Sato and T.-S. H. Lee, *J. of Phys. J.Phys. G* **36**, 73001 (2009).
  - [41] L. Heller, G.E. Bohannon, F. Tabakin, *Phys.Rev. C* **13** 742 (1976).
  - [42] T.-S. H. Lee, *Phys. Lett.* **B67**, 282 (1977).
  - [43] B. Krusche, M. Fuchs, V. Metag, M. Robig-Landau, H. Stroher, R. Beck, F. Harter and S. J. Hall *et al.*, *Eur. Phys. J. A* **6**, 309 (1999).
  - [44] P. Benz *et al.* [Aachen-Bonn-Hamburg-Heidelberg-Muenchen Collaboration], *Nucl. Phys. B* **65**, 158 (1973).
  - [45] M. Asai *et al.* [TAGX Collaboration], *Phys. Rev. C* **42**, 837 (1990).
  - [46] U. Siodlaczek, P. Achenbach, J. Ahrens, J. R. M. Annand, H. J. Arends, R. Beck, R. Bilger and H. Clement *et al.*, *Eur. Phys. J. A* **10**, 365 (2001).
  - [47] H. Gacilazo and T. Mizutani,  *$\pi NN$  System*, World Scientific (1990).
  - [48] T.-S.H. Lee and A. Matsuyama, *Phys.Rev. C* **36**, 1459 (1987)
  - [49] H. Kamano, S.X. Nakamura, T.-S. H. Lee, T. Sato, *Phys. Rev. C* **88**, 035209 (2013).
  - [50] S.X. Nakamura, H. Kamano, T. Sato, in preparation.